Applied Physics Letters

RESEARCH ARTICLE | SEPTEMBER 20 2023

Ion-implanted $Al_{0.6}Ga_{0.4}N$ deep-ultraviolet avalanche photodiodes

Hoon Jeong ; Minkyu Cho; Zhiyu Xu ; Frank Mehnke ; Nepomuk Otte ; Shyh-Chiang Shen ; Theeradetch Detchprohm ; Russell D. Dupuis

Appl. Phys. Lett. 123, 121107 (2023)
https://doi.org/10.1063/5.0161953

AIP Publishing

Applied Physics Letters ARTICLE pubs.aip.org/aip/apl

Ion-implanted $Al_{0.6}Ga_{0.4}N$ deep-ultraviolet avalanche photodiodes

Cite as: Appl. Phys. Lett. **123**, 121107 (2023); doi: 10.1063/5.0161953
Submitted: 13 June 2023 · Accepted: 28 August 2023 ·
Published Online: 20 September 2023

Hoon Jeong,[1] Minkyu Cho,[1] Zhiyu Xu,[1] Frank Mehnke,[1] Nepomuk Otte,[2] Shyh-Chiang Shen,[1] Theeradetch Detchprohm,[1] and Russell D. Dupuis[1,3,a)]

AFFILIATIONS

[1]School of Electrical and Computer Engineering, Georgia Institute of Technology, Atlanta, Georgia 30332-0250, USA
[2]School of Physics, Georgia Institute of Technology, Atlanta, Georgia 30332-0250, USA
[3]School of Material Science Engineering, Georgia Institute of Technology, Atlanta, Georgia 30332-0250, USA

[a)]**Author to whom correspondence should be addressed:** dupuis@gatech.edu

ABSTRACT

A deep-ultraviolet $Al_{0.6}Ga_{0.4}N$ *p–i–n* avalanche photodiode (APD) structure was grown on a (0001) AlN bulk substrate by metalorganic chemical vapor deposition. The wafer was fabricated into 20 μm diameter mesa APD devices both with and without ion-implantation with nitrogen ions on the periphery of the *p*-type region of the diode mesa and tested. The dark current density vs bias, photoresponse, and the optical gain of the APDs with and without ion implantation were compared. The devices fabricated with ion implantation showed improved performance, exhibiting lower dark current densities of $\sim 1 \times 10^{-9}$ A/cm^2 and a higher optical gain of $\sim 5.2 \times 10^5$ at a current density limit of 0.3 A/cm^2. The average temperature coefficients of the reverse-bias breakdown voltage were also compared. Although the data showed negative coefficients for APDs fabricated both with and without ion implantation, the ion-implanted APDs showed an improvement relative to the devices fabricated without ion-implantation.

Deep-ultraviolet (DUV) avalanche photodiodes (APDs) are photodetectors designed to measure intensities of DUV light that are too low to be detected with regular photodetectors. Ideally, with certain measurement configurations, properly designed APDs can detect single photons. With this ability, DUV APDs have several potential applications such as quantum-key distribution,[1] optical time-domain reflectometry,[2] positron-emission tomography,[3] and non-line-of-sight optical communications.[4] For such applications, arrays of UV-enhanced silicon APDs, commonly referred to as silicon photomultipliers (SiPMs), have generally been utilized with DUV filters at various wavelengths.[5]

DUV APDs fabricated from the aluminum gallium nitride ($Al_xGa_{1-x}N$) material system are candidates for the replacement of UV-enhanced SiPMs. While AlGaN APDs have been studied and developed for decades to improve the quality of the epitaxial growth and the device fabrication techniques, much work remains to be done in order for AlGaN APDs to compete in performance with SiPMs. However, AlGaN alloys have a direct bandgap energy which is tunable from 3.4 to 6.2 eV, which gives them an intrinsic capability to operate in the solar-blind spectrum at wavelengths $\lambda < 280$ nm.[6] For $Al_xGa_{1-x}N$ alloys in which the aluminum nitride (AlN) mole fraction, x, exceeds the value 0.5, the ratio of the hole, β, to electron, α, ionization coefficient, $k = \beta/\alpha$, has a value below 1, which makes the excess noise factor $F(M)$ to decrease.[7] Since $\beta < \alpha$, an electron-initiated multiplication process is preferred, thus, in this case, illumination from the *p*-side is more preferred.

In our previous report,[8] we grew $Al_xGa_{1-x}N$ *p–i–n* APDs with $x = 0.6$ on different substrates with different dislocation densities. From this study, we observed that the dislocation densities were strongly related to the leakage current density. Higher dislocation densities originating from a larger lattice mismatch of the AlGaN device layers and the AlN/sapphire or AlGaN/sapphire templates resulted higher leakage currents, as well as a lower yield of good devices down to ~5%. When the AlGaN APDs were grown on low-dislocation-density (0001) AlN bulk substrates, the leakage current densities were reduced, and the yield of good devices was relatively higher (~15%) than that of the APDs grown on AlN/sapphire templates. Recently, we studied the temperature dependence of the breakdown voltage for $Al_xGa_{1-x}N$ $x \sim 0.6$ APDs in order to evaluate the avalanche breakdown processes involved in optical gain.[3]

In addition to the improvements in device performance due to the use of high-quality substrates for lower dislocation densities to

suppress leakage currents, there have been several III-nitride materials growth and device fabrication techniques developed in previous work. In the aspect of improved growth processes, e.g., Liu, *et al.* reported the reduction in leakage currents by optimizing the minimum pressure of metalorganic chemical vapor deposition (MOCVD) growth.[9] There have also been many reported APD fabrication approaches to reduce the leakage current densities such as plasma-treatment,[10] ledged surface depletion technique,[11] photo-electrochemical treatment,[12] and deposition of various passivation layers.[13] We also earlier reported GaN UV-APDs with ion-implantation isolation methods to effectively suppress surface leakage currents.[14]

In this work, we demonstrate improved performance of $Al_xGa_{1-x}N$ *p–i–n* DUV APDs with $x = 0.6$ fabricated using an ion-implantation isolation technique. The front-illuminated AlGaN DUV APD structure was grown on a commercially available 1-in. diameter *c*-plane oriented (0001) bulk AlN substrate using an AIXTRON 3 × 2 in. close-coupled showerhead metalorganic chemical vapor deposition (MOCVD) reactor. The x-ray diffraction (XRD) FWHM of (002) and (102) ω-scans of the AlN bulk substrate were ∼24 and ∼43 arc sec, and the estimated dislocation density was below $\sim 10^3\,cm^{-3}$.[15] The growth was made using the group III precursors trimethylaluminum (TMAl) and trimethylgallium (TMGa) and the group V precursor, ammonia (NH_3). Silane (SiH_4) and bis-cyclopentadienyl magnesium (Cp_2Mg) were used for *n*-type and *p*-type dopants, respectively.

From the top, the APD structures consisted of a 20 nm-thick heavily doped *p*-GaN Mg-doped layer ([Mg] $\sim 1 \times 10^{20}\,cm^{-3}$) for Ohmic contact formation, followed by a Mg-doped 20 nm-thick *p*-$Al_xGa_{1-x}N$ grading layer ($p \sim 7 \times 10^{17}\,cm^{-3}$) with a linearly graded AlN mole fraction from $x = 0.1$ (top) to $x = 0.6$ (bottom). Next was a Mg-doped 50 nm-thick *p*-$Al_{0.6}Ga_{0.4}N$ layer, followed by a 160 nm-thick unintentionally doped (uid-layer) $Al_{0.6}Ga_{0.4}N$ absorption/multiplication layer, which had a cutoff wavelength of ∼250 nm [Fig. 1(a)]. Next was a silicon-doped 250 nm-thick *n*-$Al_{0.6}Ga_{0.4}N$ layer ($n \sim 5 \times 10^{18}\,cm^{-3}$), followed by a silicon-doped 500 nm-thick *n*-$Al_{0.75}Ga_{0.25}N$:Si layer ($n \sim 5 \times 10^{18}\,cm^{-3}$). Finally, there was a 200 nm-thick unintentionally doped $Al_{0.75}Ga_{0.25}N$ layer and a 200 nm-thick unintentionally doped $Al_{0.8}Ga_{0.2}N$ layer [Fig. 1(b)]. X-ray diffraction (XRD) reciprocal- space mapping (RSM) around the (105) reflection was used to determine the AlN mole fraction of AlGaN layers and to analyze the crystalline quality.[16] To analyze the surface morphology of the epitaxial layers, atomic-force microscopy (AFM) was used.

After the growth of the epitaxial layers, a portion of the wafer was processed for ion-implantation. The mesa regions were patterned with an SiO_2 mask and selectively implanted at 300 K with nitrogen ions on the mesa peripheries. The N-ion implantation energy was 20 keV at a 1×10^{13} ions/cm^2 dose, which created a highly resistive region[14] [Fig. 2(a)]. In the ion-implanted region, the electric fields are terminated and, thus, suppress undesirable sidewall current leakage paths.[10] Then using RIE-ICP with a BCl_3/Cl_2 plasma, the epitaxial layers were etched until the *n*-$Al_{0.75}Ga_{0.25}N$ surface was revealed while maintaining about few-hundred-microns-wide implanted region as a mesa sidewall. Using an electron-beam evaporator, vanadium-based *n*-type metal stacks (V/Al/Ti/Au)[17] were deposited on the *n*-type surface and

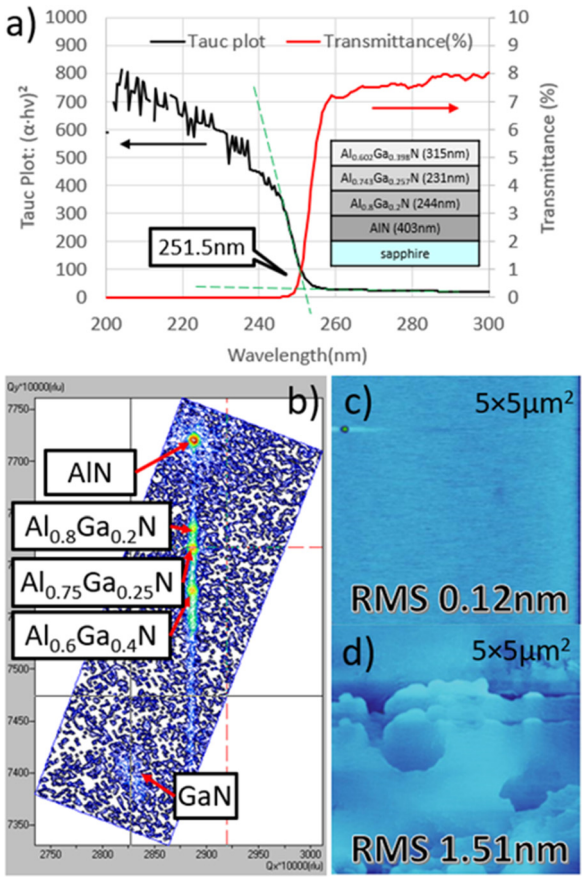

FIG. 1. (a) Tauc plot (black line) and transmittance (red line) curve of the APD sample without *p*-GaN and *p*-AlGaN composition-graded layer is shown. It is possible to derive the wavelength at the intersection of two tangent lines of the Tauc plot, which was ∼251.5 nm for $Al_{0.602}Ga_{0.398}N$. (b) X-ray diffraction (XRD) reciprocal space mapping (RSM) around the (105) reflection of the AlGaN APD heterostructure grown on the AlN bulk substrate and the analysis of the AlN mole fraction of each of the AlGaN layers. (c) Atomic-force microscopy (AFM) image of the surface of the AlN bulk substrate (b) before and (c) after the AlGaN APD grown. The RSM value of roughness before and after the growth increased from 0.123 to 1.51 nm.

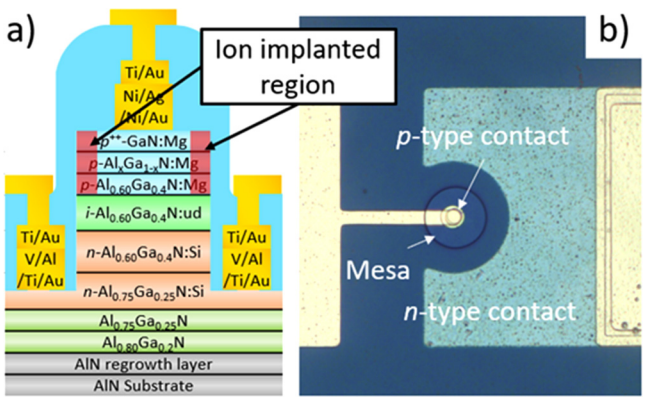

FIG. 2. Schematic diagrams of the cross section of (a) the AlGaN APDs fabricated with ion-implantation and (b) an optical microscopic image of the fabricated AlGaN APD with a circular diameter of 20 μm.

annealed at 700 °C in a N_2 ambient. Nickel-based *p*-type metal stacks (Ni/Ag/Ni/Au) were deposited on the *p*-type surface, and annealing was performed at 500 °C in a compressed dry air ambient. A 600 nm-thick SiO_2 layer passivated the AlGaN surface with plasma-enhanced chemical vapor deposition, and via holes were etched to reveal the *n*-type and *p*-type metals. Finally, 500 nm-thick Ti/Au metal stacks were deposited for wire bonding as shown in Fig. 2. Except for the implantation step, the non-implanted APDs were processed simultaneously with the same mask layout.

The *J*–*V* characteristics of the AlGaN APD devices (both non-ion-implanted and ion-implanted) were measured at various temperatures with a Keithley 4200 semiconductor characterization system. A Newport Apex Illuminator installed with an ozone-free xenon lamp and a Newport Cornerstone 260 Monochromator system, which has a spectral resolution of 2.5 nm, was used to illuminate the APDs at a wavelength of 250 nm to measure the UV photocurrent.

Figures 3(a) and 3(b) show the comparison of the current density (a) and the gain (b) vs reverse bias of a 20 μm-diameter AlGaN DUV APD device without[8] and with ion-implantation. The wafer having devices fabricated without ion-implantation had a yield of "low-leakage" devices of ~15%, whereas the wafer with ion-implanted APDs had a yield of more than 90% and the dark leakage current density was lower. In addition, the ion-implanted devices could be operated at a higher current density without damage. (The current compliance was set to 0.3 A/cm^2, which was one order magnitude higher than that of the unimplanted devices.) Both types of devices had breakdown voltages around a reverse bias of −140 V as intended. The method to determine the breakdown voltage was explained in our previous report.[8] The dark leakage current density of the devices fabricated without ion-implantation was around $\sim 1 \times 10^{-8}$ A/cm^2 until the reverse bias reached −40 V,[8] whereas the ion-implanted devices had a dark current density one order of magnitude lower $\sim 1 \times 10^{-9}$ A/cm^2. As stated in our previous paper,[10] the ion implantation can terminate the electric field at the periphery of the device, thereby minimizing sidewall leakage paths, which are enhanced by field-induced and trap-assisted generation. The maximum optical gain was determined for a current limit of 0.3 A/cm^2 for the ion-implanted APDs and 0.03 A/cm^2 for the unimplanted APDs. The maximum calculated gain of the APDs with ion-implantation was $\sim 5.27 \times 10^5$, which was 20 times higher than that of the device without ion-implantation, i.e., 2.43×10^4.[8] The gain was calculated assuming that the net photocurrent is obtained by subtracting the dark current from the measured photocurrent, which is divided by the difference between the dark and photocurrent at 0 V bias. For the optical gain calculation, the following equation was used:

$$G(V) = \frac{I_{photo}(V) - I_{dark}(V)}{I_{photo}(V=0) - I_{dark}(V=0)},$$

where $I_{photo}(V)$ and $I_{dark}(V)$ are the photocurrent/dark current in the entire reverse bias range, respectively, and $I_{photo}(V=0)$ and $I_{dark}(V=0)$ are photocurrent/dark current at a reverse bias of 0 V. From these results, it is evident that the ion-implantation reduces sidewall leakage current paths, which results in higher device yield and gain.

For the UV photoresponse measurements, UV light emitted from a 250 nm DUV light emitting diode (LED) was filtered with a 1/2-inch diameter filter with a 10 nm FWHM bandpass and illuminates the AlGaN DUV APD devices with 100 μm diameter.[8]

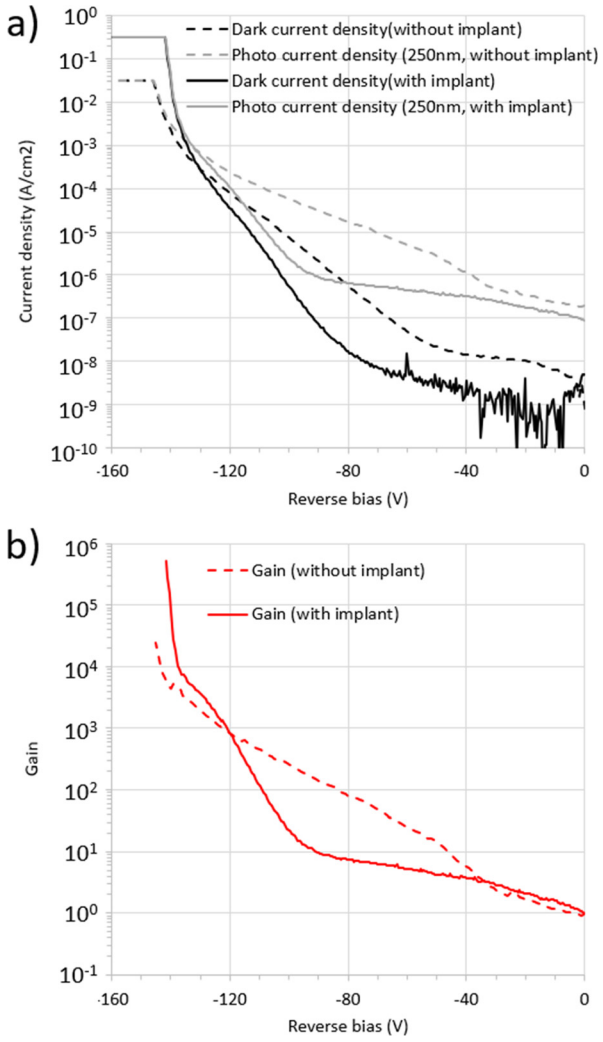

FIG. 3. (a) The dark current density (black curve) and photocurrent (gray curve) density of an AlGaN DUV APD device (20 μm diameter) with ion-implantation (solid line) and without ion-implantation[8] (dashed line), and (b) the calculated gain is also shown. The APDs were both grown on the same AlN bulk substrate.

The DUV LED was connected to a MOSFET and modulated by 125 Hz frequency rectangular pulse train. The AlGaN DUV APD was connected to a Stanford Research System 830 lock-in amplifier, which collected the photocurrent with the 1/*f* noise removed. A Si photodiode was utilized to calibrate the optical power of the UV light emitting from the LED by measuring the photocurrent. Then the 300 K photocurrent from five of the AlGaN DUV APDs was measured at zero bias, and the average photoresponse was calculated at 250 nm. For the devices without ion implantation, the average photoresponse was 71.45 ± 2.87 mA/W,[8] and for the devices with ion implantation, the average was 68.07 ± 3.20 mA/W. The equivalent external quantum efficiency was 35.43% and 33.76%.

Although the devices without ion implantation had a slightly higher photoresponse compared to the devices with ion implantation, the error range of photoresponse of the devices without ion

implantation overlapped significantly with that of the devices with ion implantation. Still, the average photoresponse measured from the devices with ion implantation was higher than that of the devices from prior reports of other institutes, which was ~60 mA/W.[18]

To understand the contributions of the avalanche process to the breakdown behavior, the temperature coefficient of the breakdown voltage of the AlGaN APDs with and without ion implantation were measured. This was done by measuring the slope of the breakdown voltage as a function of temperature (ΔV at breakdown)/ΔT. It is well understood that a positive temperature coefficient of the breakdown voltage in a p–n junction occurs when the breakdown is contributed primarily from avalanching, and it is negative when the breakdown is primarily contributed from tunneling or possibly some combination of these processes.[19] Five 20 μm-diameter AlGaN DUV APDs were selected at random, and the dark current at five temperature set points was measured, from 25 to 79 °C by steps of 13.5 °C, and the temperature coefficient of the breakdown voltage was calculated and plotted (Fig. 4). The average of the temperature coefficient of the breakdown voltage for the AlGaN APD devices without ion implantation was -0.069 ± 0.009 V/K,[8] and for the devices with ion implantation it was -0.052 ± 0.005 V/K. There was a slight increase (toward a positive value) of ~25% in the temperature coefficient for the ion-implanted APDs. Additional research needs to be done to determine if ion implantation can contribute more significantly to the improvement of the temperature coefficient of the breakdown voltage and the avalanche gain for AlGaN DUV APDs.

In summary, we reported an $Al_{0.6}Ga_{0.4}N$ DUV p–i–n APD structure grown on a (0001) AlN bulk substrate and the characteristics of APDs fabricated with and without ion implantation in the periphery of the 20 μm-dia. mesa devices. The lowest dark leakage current density at a -40 V reverse bias for the devices fabricated with ion implantation was $\sim 1 \times 10^{-9}$ A/cm^2, an improved performance by one order of magnitude compared to the similar devices fabricated without ion implantation. The maximum optical gain of the devices with ion implantation showed a superior performance of $\sim 5.2 \times 10^5$, which was 20 times higher than that of the devices without ion implantation. Moreover, the devices fabricated with ion implantation could be operated at 10×larger reverse-bias current density, and the APDs were more robust in terms of yield of low-leakage devices which was over 90%. The average UV photoresponse at 250 nm for the devices fabricated with ion implantation was ~68.07 mA/W, which was 5% lower than the average of the devices without ion implantation but within our typical range of values. The temperature coefficient of the breakdown voltage of the devices with ion implantation was still a negative value of −0.052, but there was slight improvement compared to the devices without ion implantation.

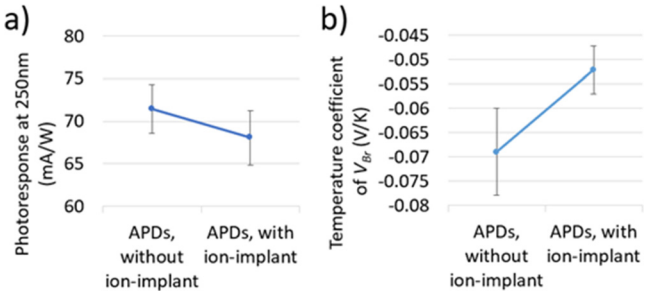

FIG. 4. (a) The plot of average and error of photoresponse at 250 nm of the AlGaN DUV APD devices with and without ion implantation are shown. Note that the error range overlapped significantly with each other. (b) The temperature coefficients of the breakdown voltage of the devices with[8] and without ion implantation were calculated from the dark current density at various temperature set points.

This work was supported in part by the U.S. Department of Energy (Dr. H. Marsiske) under No. DE-SC0019133 and the U.S. Army Research Office (Dr. M. Gerhold) under No. W911NF-15-1-0489. R. D. Dupuis acknowledges the support of the Steve W. Chaddick Endowed Chair in Electro-Optics. This work was performed in part in the facilities of the Georgia Tech Institute for Electronics and Nanotechnology, a member of the National Nanotechnology Coordinated Infrastructure, which is supported by the National Science Foundation (Grant No. ECCS-154217). The views and conclusions contained in this document are those of the authors and should not be interpreted as representing the official policies, either express or implied, of DoE, ARO, NSF, or the U.S. Government.

AUTHOR DECLARATIONS

Conflict of Interest

The authors have no conflicts to disclose.

Author Contributions

Hoon Jeong: Conceptualization (equal); Data curation (equal); Formal analysis (equal); Investigation (equal); Methodology (equal); Writing – original draft (equal). **Minkyu Cho:** Formal analysis (equal); Methodology (equal). **Zhiyu Xu:** Formal analysis (supporting); Methodology (equal). **Frank Mehnke:** Formal analysis (supporting); Methodology (supporting). **Nepomuk Otte:** Formal analysis (supporting); Funding acquisition (lead); Investigation (equal); Project administration (equal). **Shyh-Chiang Shen:** Formal analysis (supporting); Funding acquisition (equal); Investigation (equal); Project administration (equal). **Theeradetch Detchprohm:** Conceptualization (equal); Formal analysis (equal); Funding acquisition (equal); Investigation (equal); Methodology (equal); Writing – review & editing (equal). **Russell D. Dupuis:** Conceptualization (equal); Formal analysis (equal); Investigation (equal); Project administration (equal); Writing – review & editing (equal).

DATA AVAILABILITY

The data that support the findings of this study are available from the corresponding author upon reasonable request.

REFERENCES

[1]N. Gisin, G. Ribordy, W. Tittel, and H. Zbinden, Rev. Mod. Phys. **74**, 145 (2002).
[2]A. L. Lacaita, P. A. Francese, S. D. Cova, and G. Riparmonti, Opt. Lett. **18**, 1110 (1993).
[3]V. Spanoudaki, A. Mann, A. Otte, I. Konorov, I. Torres-Espallardo, S. Paul, and S. Ziegler, J. Instrum. **2**, P12002 (2007).
[4]Z. Xu and B. M. Sadler, IEEE Commun. Mag. **46**, 67 (2008).
[5]D. Kuleshov, V. Simonyan, A. Bogdanov, E. Kholupenko, Y. V. Tuboltsev, Y. V. Chichagov, and A. Krassilchtchikov, paper presented at the J. Physics: Conf. Series, 25–26 March, Coimbatore, India, 2021.

[6]H. Morkoc, *Handbook of Nitride Semiconductors and Devices* (Wiley, 2008).
[7]S. Miller and R. J. McIntyre, *Optical Fiber Telecommunications* (Elsevier, 1979); R. J. McIntyre, IEEE Trans. Electron Dev. **19**, 703 (1972).
[8]Data in Figs. 3(a) and 3(b) and Figs. 4(a) and 4(b) for AlGaN UV APDs without implant are replotted data from our prior paper: H. Jeong, M. Cho, Z. Xu, F. Mehnke, M. Bakhtiary-Noodeh, T. Detchprohm, S.-C. Shen, N. Otte, and R. D. Dupuis, J. Appl. Phys. **131**, 103102 (2022).
[9]W. Liu, D. Zhao, X. Sun, S. Zhang, D. Jiang, H. Wang, S. Zhang, Z. Liu, J. Zhu, and Y. Wang, J. Phys. D: Appl. Phys. **42**, 015108 (2009).
[10]B.-S. Zheng, P.-Y. Chen, C.-J. Yu, Y.-F. Chang, C.-L. Ho, M.-C. Wu, and K.-C. Hsieh, IEEE Electron Device Lett. **36**, 932 (2015).
[11]Y. Zhang, S.-C. Shen, H. J. Kim, S. Choi, J.-H. Ryou, R. D. Dupuis, and B. Narayan, Appl. Phys. Lett. **94**, 221109 (2009).
[12]Z. G. Shao, D. J. Chen, H. Lu, R. Zhang, W. J. Luo, Y. D. Zheng, L. Li, and Z. H. Li, IEEE Electron Device Lett. **35**, 372 (2014).
[13]W. Tan, M. Uren, P. Houston, R. Green, R. Balmer, and T. Martin, IEEE Electron Dev. Lett. **27**(1), 1 (2006); Z. Liu, G. Ng, H. Zhou, S. Arulkumaran, and Y. K. T. Maung, Appl. Phys. Lett. **98**, 113506 (2011).
[14]M. Cho, Z. Xu, M. Bakhtiary-Noodeh, H. Jeong, C.-W. Tsou, T. Detchprohm, R. D. Dupuis, and S.-C. Shen, IEEE Trans. Electron Devices. **68**, 2759 (2021).
[15]Z. Bryan, I. Bryan, J. Xie, S. Mita, Z. Sitar, and R. Collazo, Appl. Phys. Lett. **106**, 142107 (2015).
[16]V. Voronenkov, R. Gorbunov, A. Tsyuk, P. Latyshev, Y. Lelikov, Y. Rebane, A. Zubrilov, N. Bochkareva, and Y. Shreter, ECS Trans. **35**, 91 (2011).
[17]J. H. Wang, S. Mohney, S. Wang, U. Chowdhury, and R. Dupuis, J. Electron. Mater. **33**, 418 (2004).
[18]P. Reddy, M. Hayden Breckenridge, Q. Guo, A. Klump, D. Khachariya, S. Pavlidis, W. Mecouch, S. Mita, B. Moody, and J. Tweedie, Appl. Phys. Lett. **116**, 081101 (2020).
[19]M. S. Tyagi, Solid-State Electron. **11**, 99 (1968).